Wolf-Rayet Stars
W.-R. Hamann, A. Sander, H. Todt, eds.
Potsdam: Univ.-Verlag, 2015
URL: http://nbn-resolving.de/urn:nbn:de:kobv:517-opus4-84268

X-ray Emission from Ionized Wind-Bubbles around Wolf-Rayet Stars

V. V. Dwarkadas[1] & D. Rosenberg[2]
[1] *Astronomy and Astrophysics, University of Chicago*
[2] *Oak Ridge National Laboratory*

Using a code that employs a self-consistent method for computing the effects of photoionization on circumstellar gas dynamics, we model the formation of wind-driven nebulae around massive Wolf-Rayet (W-R) stars. Our algorithm incorporates a simplified model of the photo-ionization source, computes the fractional ionization of hydrogen due to the photoionizing flux and recombination, and determines self-consistently the energy balance due to ionization, photo-heating and radiative cooling. We take into account changes in stellar properties and mass-loss over the star's evolution. Our multi-dimensional simulations clearly reveal the presence of strong ionization front instabilities. Using various X-ray emission models, and abundances consistent with those derived for W-R nebulae, we compute the X-ray flux and spectra from our wind bubble models. We show the evolution of the X-ray spectral features with time over the evolution of the star, taking the absorption of the X-rays by the ionized bubble into account. Our simulated X-ray spectra compare reasonably well with observed spectra of Wolf-Rayet bubbles. They suggest that X-ray nebulae around massive stars may not be easily detectable, consistent with observations.

1 Introduction:

Massive stars (> 8 M$_\odot$) lose mass throughout their lifetime, via winds and eruptions, before ending their lives in a cataclysmic supernova (SN) explosion. The interaction of this material with the surrounding medium creates vast wind-blown cavities surrounded by a dense shell, referred to as wind-blown bubbles. As the star evolves through various stages, the mass-loss parameters will change, affecting the structure of the bubble. When the star finally explodes, the resulting SN shock wave will expand within the bubble, and the dynamics and kinematics of the shock wave will depend on the bubble parameters (Dwarkadas 2005, 2007a,b). Similarly, the relativistic blast waves associated with gamma-ray bursts are expected to expand within wind bubbles surrounding Wolf-Rayet (W-R) stars. Using an ionization-gasdynamics code, AVATAR, we compute the structure and evolution of the wind-blown bubbles around massive stars. Using the ISIS package, we compute the X-ray spectrum from the simulations as would be observed by the Chandra satellite, and compare to observational data.

2 The AVATAR Code:

We have further developed a code that combines photoionization from the star with the gasdynamics, and used it to compute the structure of wind bubbles around massive stars. The method operator splits the contribution due to photoionization effects from the usual gas dynamics, and utilizes a backward-Euler scheme together with a Newton-Raphson iteration procedure for achieving a solution. The effects of geometrical dilution and of column absorption of radiation are considered. The gasdynamic algorithm makes use of a multidimensional covariant implementation of well established Eulerian finite difference algorithms (Rosenberg 1995). A second-order (van Leer) monotonic transport algorithm is used for advection of total mass and the neutral component, and a third order piecewise parabolic scheme is available. Tabulated functions are used to compute the collisional ionization rate and cooling function. Shocks are treated using an artificial viscosity. Grid expansion is available to study flow over distance scales spanning several orders of magnitude. The algorithm incorporates a simplified model of the photo-ionization source, computes the fractional ionization of hydrogen due to the photo-ionizing flux and recombination, and determines self-consistently the energy balance due to ionization, photo-heating and radiative cooling. In this, our method is superior to that of other calculations, such as Garcia-Segura et al. (1996); van Marle et al. (2005), who use the on-the-spot approximation and do not take the recombination time into account. It is comparable to the work of Toalá & Arthur (2011).

3 Evolution of the Wind-Blown bubble around a 40 M$_\odot$ star:

A model for a 40 $M_\odot$ star using the AVATAR code is shown in Figure 1. Stellar parameters are adapted from van Marle et al. (2005). The evolution of the star can be divided into 3 main phases. An inhomogeneous pressure and density distribution develops in the main-sequence (MS) stage, accompanied by vorticity deposition near the inner shock. The inclusion of photo-ionization results in the formation of a dense, lower temperature ($\sim 10^4$ K) region of ionized material outside the wind bubble during the

MS phase. The nebula is fully ionized, and the ionization front is trapped in the dense shell, which is unstable to ionization instabilities. In the red supergiant (RSG) stage the surface temperature of the star decreases considerably. Consequently the ionizing radiation drops considerably and recombination reduces the ionization fraction to $\sim 40\%$, although this goes up again in the W-R stage. The high-density RSG wind is followed by a higher momentum W-R wind which breaks up the RSG shell, scattering the dense material into a turbulent W-R nebula.

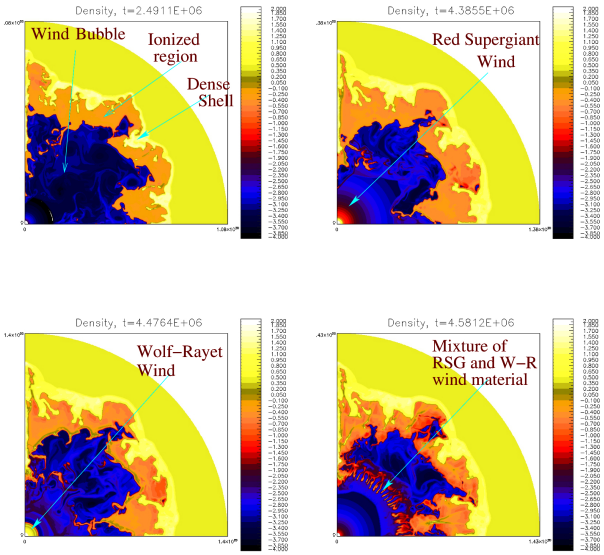

Fig. 1: Density snapshots from calculation of wind bubble evolution around 40 $M_\odot$ star (600 × 400 zones), computed with AVATAR with expanding grid (Dwarkadas & Rosenberg 2013). Time increases from left to right and top to bottom, and is listed at the top of each plot.

We can use the simulations to illustrate the regions from which the X-ray flux arises. We assume that thermal bremsstrahlung is the dominant contributor to the X-ray flux, although line emission will also play a role. The flux is then proportional to $n_e^2 T^{1/2}$ where n_e is the density and T the temperature. We show maps of this quantity at various times in Figure 2. The normalization is arbitrary, however they are all normalized to the same scale. Only zones having temperature $T > 10^6$ K are assumed to emit X-rays. The densest clumps do not contribute because their temperature is lower than 10^6 K. It is clear that the highest X-ray flux arises in the W-R stage, and that the highest levels of X-ray emission emanate from very small regions.

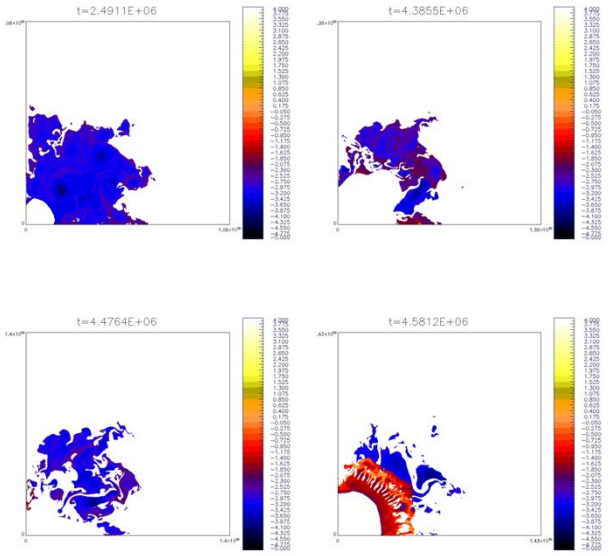

Fig. 2: Maps showing the area from which X-ray emission arises from the bubble in Figure 1. An increase of the X-ray flux in the W-R stage is seen.

4 THE X-RAY SPECTRUM OF THE BUBBLE:

In order to calculate the X-ray emission accurately, we use the ISIS package (Houck & Denicola 2000). The data are read into ISIS, the spectrum calculated for every zone, taking the absorption outside that zone into account, and added together. A point source is assumed. We use the VMEKAL model in XSPEC to model the spectrum, since it is the one most commonly used to fit the observed X-ray spectra. Herein we present (Figure 3) X-ray spectra as would be detected by the Chandra ACIS instrument for an object at 1.5kpc distance, integrated over 50,000s. Foreground absorption of 2×10^{20} cm^{-2} is added to absorption due to the neutral material surrounding the bubble, which varies, and can be as high as 2×10^{21} cm^{-2} (total $N_{\rm H}$ in units of 10^{22} cm^{-2}). Line broadening is based on the underlying fluid velocity. Solar abundances (Anders & Grevesse 1989) are used for the MS and RSG stages. Abundances in the W-R phase are from Chu et al. (2003) for the W-R bubble S308.

Our spectra are comparable in shape and temperature to observed spectra (Figure 4). Our simulations show that the X-ray emission in the MS phase is generally too weak to be detected by current X-ray satellites. It is higher in the W-R stage, but still difficult to detect. The X-ray emission depends strongly on the density within the bubble, which is a function of the density of the material around the

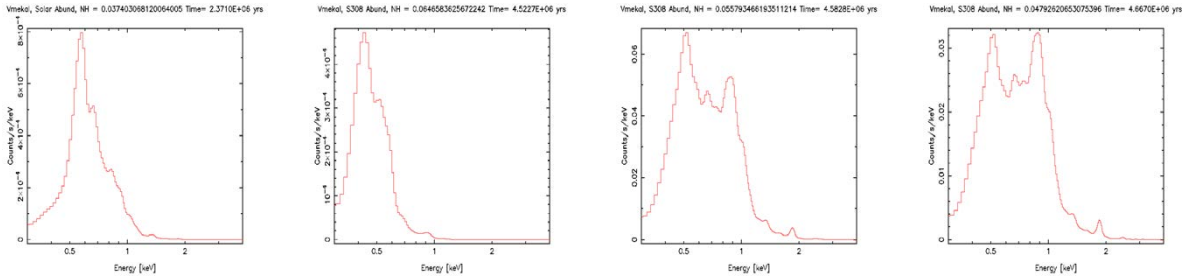

Fig. 3: Simulated X-ray spectra for a point source calculated from the simulation shown in Figure 1. The leftmost image is from the MS phase, the next three are from the W-R phase. Note that as time increases in the W-R stage, the intensity of the spectrum (counts/sec/keV) also increases.

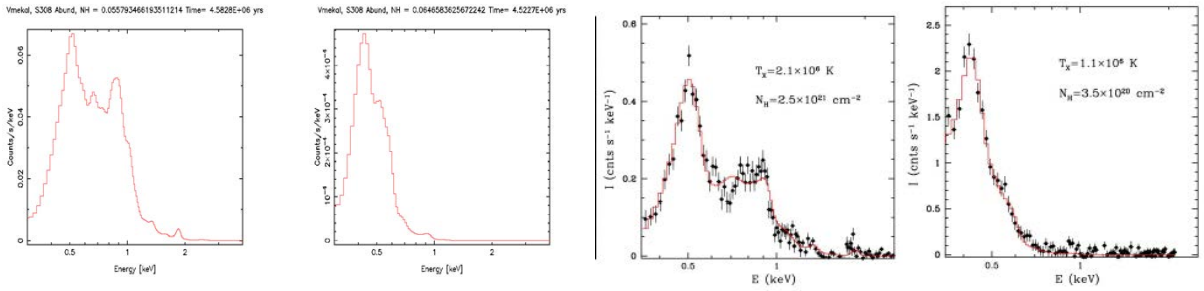

Fig. 4: Simulated and Observed spectra. Panel 1 resembles observed Chandra spectrum for NGC 6888 (panel 3) and Panel 2 XMM spectrum of S308 (panel 4), from Chu et al. (2006). Although the spectral shapes are similar, the counts are significantly lower in our simulated spectra as compared to the data. This seems to be generally true over all our simulations, in agreement with the fact that diffuse X-ray emission is not generally observed.

nebula. Thus it is possible that a higher ambient density leads to a higher intensity, although unless it was all ionized the absorption would correspondingly increase. The general low intensity is in agreement with observations, which have only detected 3 W-R nebulae, and no MS nebulae around massive stars (Chu et al. 2006; Toalá et al. 2014, 2015).

Acknowledgements: Support for VVD is provided by Chandra grants TM9-0001X and TM5-16001X issued by the CXO, which is operated by SAO for and on behalf of NASA under contract NAS8-03060. DR acknowledges resources of the OLCF at ORNL, which is supported by the Office of Science of the U.S. DOE under Contract No. DE-AC05-00OR22725.

References

Anders, E. & Grevesse, N. 1989, Geochim. Cosmochim. Acta, 53, 197

Chu, Y.-H., Gruendl, R. A., & Guerrero, M. A. 2006, in ESA Special Publication, Vol. 604, The X-ray Universe 2005, ed. A. Wilson, 363

Chu, Y.-H., Guerrero, M. A., Gruendl, R. A., García-Segura, G., & Wendker, H. J. 2003, ApJ, 599, 1189

Dwarkadas, V. V. 2005, ApJ, 630, 892

Dwarkadas, V. V. 2007a, in Revista Mexicana de Astronomia y Astrofisica Conference Series, Vol. 30, 49–56

Dwarkadas, V. V. 2007b, ApJ, 667, 226

Dwarkadas, V. V. & Rosenberg, D. L. 2013, High Energy Density Physics, 9, 226

Garcia-Segura, G., Langer, N., & Mac Low, M.-M. 1996, A&A, 316, 133

Houck, J. C. & Denicola, L. A. 2000, in Astronomical Society of the Pacific Conference Series, Vol. 216, Astronomical Data Analysis Software and Systems IX, ed. N. Manset, C. Veillet, & D. Crabtree, 591

Rosenberg, D. L. 1995, PhD thesis, The University of North Carolina at Chapel Hill

Toalá, J. A. & Arthur, S. J. 2011, ApJ, 737, 100

Toalá, J. A., Guerrero, M. A., Chu, Y.-H., & Gruendl, R. A. 2015, MNRAS, 446, 1083

Toalá, J. A., Guerrero, M. A., Gruendl, R. A., & Chu, Y.-H. 2014, AJ, 147, 30

van Marle, A. J., Langer, N., & García-Segura, G. 2005, A&A, 444, 837

Anthony Marston: Can you say how different your simulations would be if you used an LBV rather than an RSG as an intermediate phase of evolution?

Vikram Dwarkadas: The main difference in our simulations would be due to the wind properties between an LBV and a RSG. LBV wind properties are not that well defined. The wind velocities are higher than RSGs, in the range of 100–200 km/s, which means that the winds would expand further than RSG winds. However, since the density varies inversely as the wind velocity, this would reduce the density of the winds compared to the RSG phase, for equivalent mass-loss rate. Decreasing density would result in higher temperatures. The wind mass-loss rates could vary. If the mass-loss rates were equivalent then the RSG wind would be slower and more dense, and presumably more unstable. Some LBVs in eruption could achieve very high mass-loss rates, much higher than RSG wind mass-loss rates, although this would not last for a long time. This could considerably increase the total mass output in this phase. Furthermore, the momentum of the winds would be much higher, perhaps comparable to the subsequent W-R wind, which would then not be able to break up the shell easily and mix the material over the entire nebula.